Available online at www.sciencedirect.com
ScienceDirect
Atmospheric Environment 42 (2008) 1828–1845
ATMOSPHERIC ENVIRONMENT
www.elsevier.com/locate/atmosenv

Scientific uncertainties in atmospheric mercury models III: Boundary and initial conditions, model grid resolution, and Hg(II) reduction mechanism

Pruek Pongprueksa[a], Che-Jen Lin[a,b,*], Steve E. Lindberg[c,d,1], Carey Jang[e], Thomas Braverman[e], O. Russell Bullock Jr.[f], Thomas C. Ho[g], Hsing-Wei Chu[h]

[a]*Department of Civil Engineering, Lamar University, Beaumont, TX 77710, USA*
[b]*School of Environmental Science and Engineering, South China University of Technology, Guangzhou City, China*
[c]*Environmental Sciences Division, Oak Ridge National Laboratory, USA*
[d]*Department of Natural Resources and Environmental Science, University of Nevada in Reno, USA*
[e]*Office of Air Quality Planning and Standards, USEPA, Research Triangle Park, NC 27711, USA*
[f]*NOAA Air Resources Laboratory[2], Research Triangle Park, NC 27711, USA*
[g]*Department of Chemical Engineering, Lamar University, TX 77710, USA*
[h]*Department of Mechanical Engineering, Lamar University, TX 77710, USA*

Received 22 June 2007; received in revised form 11 November 2007; accepted 13 November 2007

Abstract

In this study, the model response in terms of simulated mercury concentration and deposition to boundary condition (BC), initial condition (IC), model grid resolution (12 km versus 36 km), and two alternative Hg(II) reduction mechanisms, was investigated. The model response to the change of gaseous elemental mercury (GEM) concentration from 0 to 2 ng m^{-3} in IC/BC is found to be very linear ($r^2 > 0.99$) based on the results of sensitivity simulations in July 2001. An increase of 1 ng m^{-3} of GEM in BC resulted in an increase of 0.81 ng m^{-3} in the monthly average of total mercury concentration, and 1270 ng m^{-2} in the monthly total deposition. IC has similar but weaker effects compared to those of BC. An increase of 1 ng m^{-3} of GEM in IC resulted in an increase of 0.14 ng m^{-3} in the monthly average of total mercury concentration, and 250 ng m^{-2} in the monthly total deposition. Varying reactive gaseous mercury (RGM) or particulate mercury (PHg) in BC/IC has much less significant impact. Simulation results at different grid resolutions show good agreement (slope = 0.950–1.026, r = 0.816–0.973) in mercury concentration, dry deposition, and total deposition. The agreement in wet deposition is somewhat weaker (slope = 0.770–0.794, r = 0.685–0.892) due to the difference in emission dilution and simulated precipitation that subsequently change reaction rates in the aqueous phase. Replacing the aqueous Hg(II)-HO_2 reduction by either RGM reduction by CO (5×10^{-18} cm^3 $molecule^{-1}$ s^{-1}) or photoreduction of RGM (1×10^{-5} s^{-1}) gives significantly better model agreement with the wet deposition measured by Mercury Deposition Network (MDN). Possible ranges of the reduction rates are estimated based on model sensitivity results. The kinetic estimate requires further verification by laboratory studies.

Keywords: Atmospheric mercury; Boundary and initial conditions; CMAQ-Hg; Grid resolution; Mercury reduction mechanism

*Corresponding author at: Department of Civil Engineering, Lamar University, 211 Redbird Lane, ML 10024, Beaumont, TX 77710, USA. Tel.: +1 409 880 8761; fax: +1 409 880 8121.
E-mail address: Jerry.Lin@lamar.edu (C.J. Lin).
[1]Now in Graeagle, CA 96103, USA.
[2]In partnership with the US Environmental Protection Agency.

1352-2310/$ - see front matter © 2007 Elsevier Ltd. All rights reserved.
doi:10.1016/j.atmosenv.2007.11.020

1. Introduction

The mercury model of Community Multiscale Air Quality modeling system (CMAQ-Hg) has been used extensively as a modeling tool for atmospheric mercury studies in North America (Bullock and Brehme, 2002; Gbor et al., 2006, 2007; Lin and Tao, 2003; Sillman et al., 2007), and for intercontinental transport (Lin et al., 2006b). Recently, Lin et al. (2006a, 2007) assessed quantitatively the model uncertainties in mercury emission processing, gaseous and aqueous chemistry, aqueous mercury speciation, dry deposition, and wet deposition through sensitivity simulations using CMAQ-Hg. In this study, the impacts of BC, IC, model grid resolution, and potentially missing chemical reactions in the models on simulated mercury concentration and deposition are investigated systematically.

Model sensitivity to BC has been studied by Pai et al. (1999) using a 3-D model, which reported a negligible effect on simulated wet deposition by varying RGM from 0 to 160 $pg\,m^{-3}$. However, since mercury deposition is primarily driven by chemistry (Lin and Pehkonen, 1999; Lin et al., 2007), it is necessary to understand the impact of GEM in BC, which is investigated in this study. Model sensitivity to IC is also included because of its importance to regional modeling. Special attention was devoted to understanding the impact caused by IC in terms of its magnitude and time period corresponding to a domain size.

On the effect of grid resolution, Pai et al. (2000) noted that short-term wet deposition results (daily or weekly variation) are more sensitive to grid resolution as opposed to long-term simulations (seasonal and annual averages). They also reported a two-fold increase in total concentration and dry deposition near major point sources when increasing the spatial resolution from 100 to 20 km. Seigneur et al. (2003) reported a poor correlation between the simulated wet deposition at a 100 km and at a 20 km resolution. The use of the finer resolution improved the model performance upwind of major emission sources, but the performance is compromised downwind (overestimation of wet deposition). They hypothesized that some key mercury chemical transformations are likely missing in the model (Seigneur et al., 2003), which leads to a greater degree of oxidation of the emitted mercury at the finer resolution. In this study, the effect of grid resolution is further investigated in two domains using 36 and 12 km. The results at 12 km resolution have not been reported in mercury modeling studies previously.

One of the uncertainties in mercury models is the treatment of Hg(II) reduction mechanism (Lin et al., 2006a). The gas-phase reduction of RGM to GEM has been reported in power plant plumes using measured concentration downwind and model estimation (Lohman et al., 2006). They proposed two possible reduction pathways of RGM: a pseudo-first-order decay with a rate of $0.3\,h^{-1}$ and a second-order reduction by SO_2 with a rate of $0.007\,ppb^{-1}\,h^{-1}$ ($8\times10^{-18}\,cm^3\,molecule^{-1}\,s^{-1}$). Seigneur et al. (2006) adopted those two pathways in a global mercury model. They tested a first-order reduction rate of $0.15\,h^{-1}$ and found that it caused unreasonably high GEM concentrations, i.e., approximately four times greater than observations. They also replaced the aqueous Hg(II) reduction HO_2 (Pehkonen and Lin, 1998; Gårdfeldt and Jonsson, 2003) with the reduction of RGM by SO_2 using a reaction rate of $8\times10^{-18}\,cm^3\,molecule^{-1}\,s^{-1}$ and found that this mechanism alone was not sufficient for producing realistic GEM concentration in the model. Other alternative reduction pathways have not been tested in regional models.

The objective of this study is to quantitatively assess the uncertainties of atmospheric mercury models caused by different grid resolutions, BC, IC, and chemical reduction mechanisms. One approach to address the uncertainty issue is to perform sensitivity simulations for quantifying the variation caused by different science implementations in models. In this study, sensitivity simulations were performed using identical emission inventory for the 12 and 36 km domains to demonstrate the effect of model grid resolution. The effect of varying GEM, RGM and PHg concentrations in BC and IC on the simulated concentration and deposition is shown. Two alternative gas-phase reduction mechanisms of RGM replacing the aqueous Hg(II) reduction by HO_2 are also tested using CMAQ-Hg. The goal is to verify whether or not implementing new reduction mechanisms would improve model performance in regional-scale modeling.

2. Methods

2.1. Model domains and grid resolutions

Two model domains were used in this study: (1) the continental United States (CONUS) domain,

and (2) the Northeast, Midwest, and South (NMAS) regional US domain, which is nested inside the CONUS domain. Both domains use a Lambert conformal projection centered at 40°N and 97°W, as shown in Fig. 1. The CONUS domain has 148×112 horizontal cells and a resolution of 36 km with 14 vertical layers (see Table 1). The NMAS has 279×240 horizontal cells with a 12 km horizontal resolution and uses the same vertical structure as the CONUS domain. The CONUS domain was used in the studies of BC and IC, grid resolution, and alternative Hg(II) reduction mechanisms, while the NMAS domain was used in the study of grid resolution only.

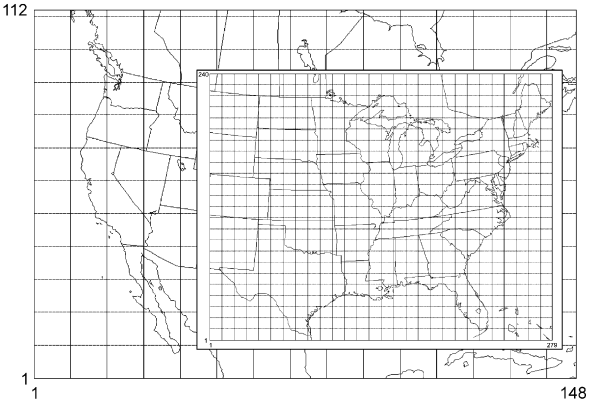

Fig. 1. The continental United State (CONUS) and the Northwest, Midwest, and South (NMAS) domain, with horizontal resolutions of 36 and 12 km, respectively.

2.2. Model input data

2.2.1. Meteorological data

The 2001 hourly meteorological fields were used for model simulations. The simulations were performed for the entire months of January and July of 2001 to represent the seasonal variation (winter and summer) of the model results. The meteorological data were prepared by the United State Environmental Protection Agency (USEPA) using a Mesoscale Meteorological Model (MM5, version 3.7) (Grell et al., 1994). The MM5 outputs were processed to the CMAQ-ready format using Meteorology-Chemistry Interface Processor (MCIP, version 3.1) as described by Byun and Ching (1999). In the MCIP processing, the dry deposition velocities (V_{dep}) of GEM and RGM were calculated using M3DRY deposition scheme (Pleim and Byun, 2004). The V_{dep} of sulfate aerosols were used as a surrogate for PHg (Bullock and Brehme, 2002).

2.2.2. Emission inventory

The emission inventory (EI) of anthropogenic mercury, criterion pollutants and other precursors was prepared using the Sparse Matrix Operator Kernel Emissions modeling system (SMOKE) version 2.2 (available from www.cmascenter.org) by the USEPA. The EI of criterion pollutants and precursors was based on the 1999 National Emission Inventory estimates (NEI99) version 3 and 2000 Canadian inventory, available from USEPA's

Table 1
Model vertical layer structure and base-case mercury species concentrations

Layer	σ_p	Height of layer top (m)	GEM (ppmV)[a] (base-case)	RGM (ppmV)[a] (base-case)	PHg ($\mu g\,m^{-3}$) (base-case)
1	0.995	36	1.780E−07	2.000E−09	1.080E−05
2	0.990	73	1.780E−07	2.000E−09	1.080E−05
3	0.980	146	1.779E−07	2.143E−09	1.072E−05
4	0.960	294	1.774E−07	2.571E−09	1.049E−05
5	0.940	445	1.769E−07	3.071E−09	1.022E−05
6	0.910	675	1.766E−07	3.429E−09	1.003E−05
7	0.860	1071	1.760E−07	4.000E−09	9.718E−06
8	0.800	1569	1.757E−07	4.333E−09	8.998E−06
9	0.740	2094	1.753E−07	4.697E−09	8.213E−06
10	0.650	2941	1.749E−07	5.093E−09	7.308E−06
11	0.550	3983	1.746E−07	5.444E−09	6.358E−06
12	0.400	5810	1.741E−07	5.907E−09	5.109E−06
13	0.200	9062	1.735E−07	6.500E−09	3.240E−06
14	0.000	14,657	1.730E−07	7.000E−09	1.620E−06

[a] $1\ ppmV = 8.20 \times 10^6\ ng\,m^{-3} = 8.20 \times 10^9\ pg\,m^{-3}$ at 1 atm, 25 °C.

ftp site (ftp.epa.gov). For anthropogenic mercury emission in the US, the point and area source emissions of NEI99 Hazardous Air Pollutant (HAP) inventory, with updates from municipal waste incinerators in 2002, were used. The Canadian mercury emission was based on the year 2000 point and non-point emission estimates (documentation available from ftp.epa.gov). The speciation of the anthropogenic emission followed the recommendations by Walcek et al. (2003). The mercury emissions from vegetation, water and soil surfaces were also included following Lin et al. (2005). The detailed mercury emission inventory and the speciation have been summarized by Lin et al. (2007). Identical EI data were gridded for both spatial resolutions (12 and 36 km).

2.2.3. Boundary and initial conditions

Boundary and initial conditions were reprojected from the outputs of a global 3-D chemical transport model (GEOS-Chem CTM, Selin et al., 2007) for both CONUS and NMAS domains except in the sensitivity simulations of BC and IC. For the BC and IC experiments of GEM, GEM concentration was varied from 0 to $2\,ng\,m^{-3}$, with $\sim 1.5\,ng\,m^{-3}$ used as the base-case for comparison. The variations were selected based on the annual mean GEM concentrations of 1.06–1.90 $ng\,m^{-3}$ over land-based sites (Selin et al., 2007). For RGM and PHg, the concentrations were set to $0\,pg\,m^{-3}$ to investigate their impact on model results. The base-case concentration of GEM, RGM, and PHg in BC and IC are shown in Table 1.

2.3. Chemical transport model

The CMAQ-Hg version 4.5.1 was used for the sensitivity simulations. The model components and relevant information have been described elsewhere (Bullock and Brehme, 2002; Lin et al., 2006a, 2007). The Carbon Bond mechanism (CB-IV) was used as the gas-phase chemical mechanism to generate the concentrations of photochemical oxidants. Rosenbrock solver (ROS3 in CMAQ CTM) was used as the chemical solver because of its flexibility (not mechanism specific). A global mass-conserving scheme (YAMO) was used for vertical and horizontal advection calculation, and the K-theory eddy diffusivity scheme was used for the vertical diffusion (documentation for the schemes is available from www.cmascenter.org).

For the sensitivity simulations with alternative Hg(II) reduction mechanisms, CMAQ-Hg 4.5.1 was modified by assigning the products of all GEM oxidation reactions (with O_3, H_2O_2, OH, and Cl) to RGM (Lin et al., 2006a, 2007) and turning off the aqueous Hg(II) reduction by HO_2 (Pehkonen and Lin, 1998; Gårdfeldt and Jonsson, 2003). Two hypothetical reduction mechanisms were implemented: RGM reduction by CO and photoreduction of RGM. RGM reduction by CO is based on an early study by Fay and Seeker (1903), which reported the reduction of mercury oxide starts at low temperature (0 °C). In addition, reduction of mercuric oxide (HgO) has been used to measure H_2 (Kawano et al., 2004, 2005) and CO (Beckman et al., 1948; McCullough et al., 1947) in the atmosphere. The reduction mechanism is believed to be (Seigneur et al., 1994):

$$HgO_{(s,g)} + CO_{(g)} \xrightarrow{k} Hg_{(g)} + CO_{2(g)} \quad (1)$$

where k is the reduction rate constant. This reaction is an exothermic reaction with an enthalpy of $-130.7\,kJ\,mol^{-1}$. A second-order rate coefficient from 10^{-20} to $10^{-14}\,cm^3\,molecule^{-1}\,s^{-1}$ was tested. The other reduction mechanism was assumed based on the photodecomposition of RGM. It is known that many Hg(II) species (e.g., $HgCl_2$, HgO, $Hg(CN)_2$, HgI_2, $HgSO_4$, HgS, etc.) are sensitive to, and can be decomposed by light (Aldrich Chemical Company, 2006). The photoreduction mechanism of RGM can be written as

$$RGM + h\nu \xrightarrow{J_{RGM}} Hg^{o}_{(g)} + \text{products} \quad (2)$$

where J_{RGM} is photoreduction rate coefficient of RGM. For model implementation, J_{RGM} is assumed to be proportional to the photolysis rate of NO_2. Similar approach was also used for the photolysis of Cl_2 (Tanaka et al., 2003):

$$J_{RGM} = f \times J_{NO_2} \quad (3)$$

where J_{NO_2} is photolysis rate coefficient of NO_2 ($\approx 10^{-2}\,s^{-1}$ at ground level) (Jacobson, 1999), f is a multiplication factor. The factor ranging from 10^{-5} to 10^{1} was tested in the simulations.

2.4. Data analysis

A suite of file operators (netCDF Operators or NCO, Zender, 2007) was used for the analysis of the CMAQ-Hg outputs. The Package for Analysis and

Visualization of Environmental data (PAVE) version 2.3 (available from www.cmascenter.org) was used for data visualization. To compare the model results at different spatial resolutions, the model results in the CONUS domain (36 km grid) were regridded into the same domain specifications as the NMAS domain (12 km grid) so that the number of data points at both grid resolutions is the same. In other words, a grid cell from the CONUS domain (36 km) will represent nine grid cells after the regridding. In the RGM reduction mechanism experiments, simulated monthly mercury wet depositions in the CONUS 36 km were compared with the MDN-measured wet deposition to estimate the possible range of the reduction rate of the proposed mechanisms.

3. Results and discussion

3.1. Model grid resolution

The simulation results at 36 and 12 km grid resolutions in July 2001 are shown in Fig. 2. The spatial distribution at both resolutions is similar for the monthly average surface mercury concentration (Fig. 2a) and the monthly mercury dry deposition (Fig. 2b). The 12 km results give a smoother texture. The distribution of mercury wet deposition (Fig. 2c) and total (dry + wet) mercury deposition (Fig. 2d) from the two resolutions are slightly different, which is caused by the difference in emission dilution and simulated precipitation of the two domains at locations near the emission sources and above oceans. Particularly, the wet deposition difference above the ocean (Fig. 2c) is primarily caused by the difference in the simulated precipitation. This leads to different aqueous concentrations of mercury and its oxidants/reductants, which subsequently influences the aqueous phase chemistry and wet deposition.

The scatter plots of 36 and 12 km simulation results in January and July are shown in Fig. 3. Each subplot consists of 71,280 data points (equal to the number of grid cells in the NMAS domain). The results from the two resolutions are highly correlated (slope = 0.995–1.026, $r = 0.864$–0.973 for mercury concentration (Fig. 3a) and dry deposition (Fig. 3b) in both months. However, the simulated mercury wet deposition at different resolutions is more scattered Fig. 3c, show some disagreements slope = 0.770–0.794, $r = 0.685$–0.892). Therefore, the simulated total deposition shows less agreement (Fig. 3d, slope = 0.950–0.958, $r = 0.816$–0.895) compared to the results of mercury concentration and dry deposition. In Fig. 3b (right, July simulation), there are two clusters of dry deposition data points falling beyond the 1:2 and 2:1 lines. Although the number of such data points only represents a small fraction of the grids, they do cause a greater degree of scattering of the total deposition data (Fig. 3d, right).

The locations where the dry deposition disagreement occurs in the domain (Fig. 3d, right) were investigated. It was found that the extreme over- and under-estimations are near water surface (Fig. 4) because of the different landuse category classification at the two grid resolutions. For example, supposed that a grid at the coastline is classified as land in the CONUS domain (36 km grid). The same grid cell is resolved into nine different grid cells in the NMAS domain (12 km grid), some of which may be classified as water at the 12 km resolution. Since the landuse category has an important impact on the magnitude of mercury V_{dep} in the summer month (Fig. 3b, right), the same location classified as land in the CONUS domain but classified as water in the NMAS domain exhibits strong underestimation in the scatter plot, and vice versa. The impact in the winter month (Fig. 3, left) is weaker because the V_{dep} is limited by aerodynamic resistance instead of canopy/surface resistance as in the summer month (Lin et al., 2006a; Abbott et al., 2008).

In general, the simulation results at the 36 and 12 km resolutions agree with each other reasonably well based on the regression statistics shown in Fig. 3. Compared to the MDN data, the simulated precipitation at both resolutions agrees with the measured precipitation (slope = 1.07, $r^2 = 0.87$ for the CONUS domain; slope = 1.01, $r^2 = 0.88$ for the NMAS domain). However, the simulated wet deposition underpredicts the measured deposition (slope = 0.66, $r^2 = 0.76$ for the CONUS domain; slope = 0.65, $r^2 = 0.75$ for the NMAS domain). It is interesting to note that the finer grid resolution does not yield a better model performance in mercury wet deposition when compared to MDN data because the MDN sites are not located near anthropogenic mercury emission sources (Fulkerson and Nnadi, 2006; Kellerhals et al., 2003; Temme et al., 2007). Therefore, the simulated wet deposition at the fine resolution is lower than the coarse resolution due to less immediate dispersion after emission and atmospheric transport to the MDN sites. A finer grid

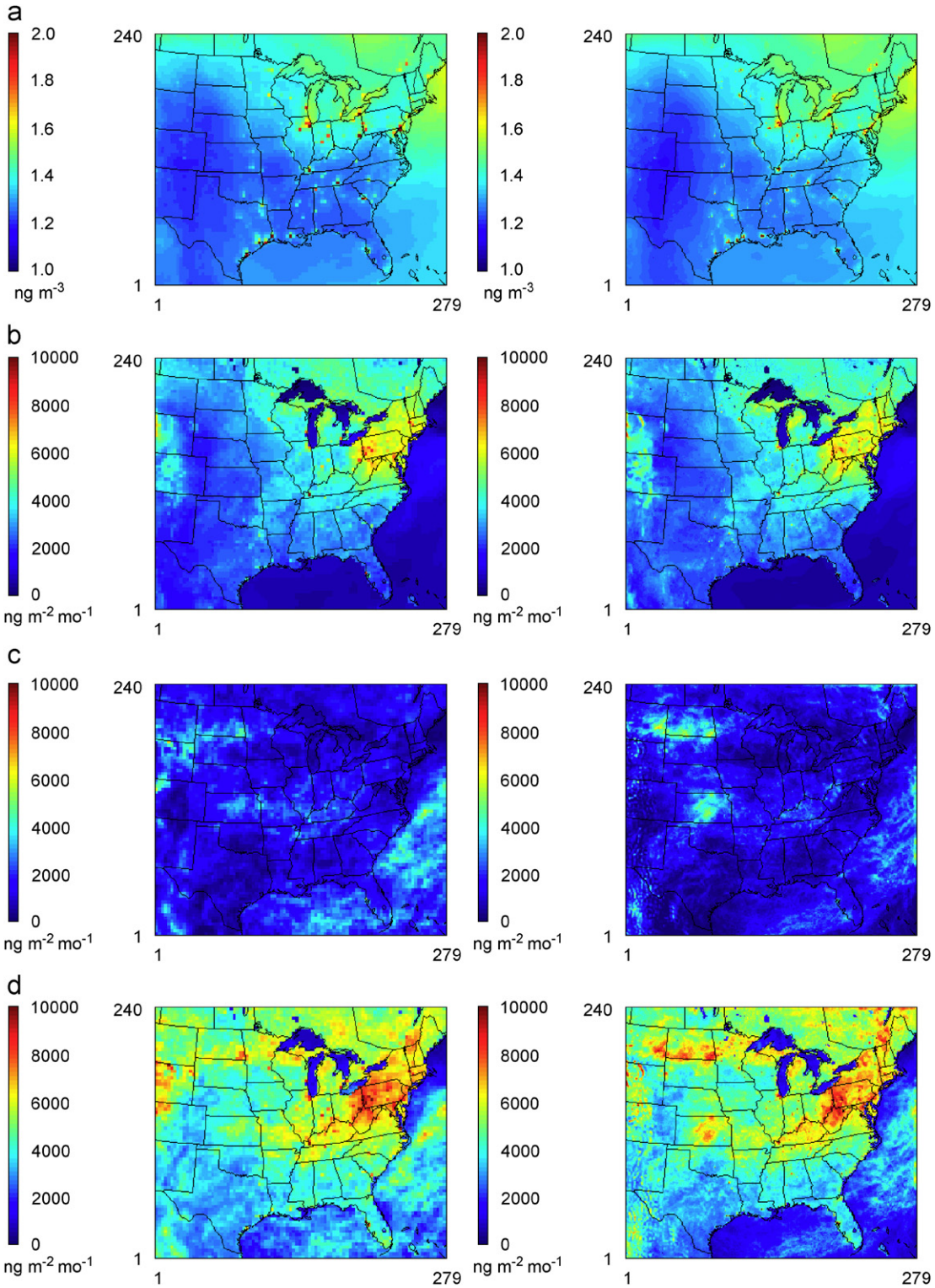

Fig. 2. Model simulation results of 36 km (left) and 12 km (right) grid resolutions for July 2001: (a) monthly average total concentration (GEM + RGM + PHg), (b) monthly accumulated dry deposition, (c) monthly accumulated wet deposition, and (d) monthly accumulated total deposition.

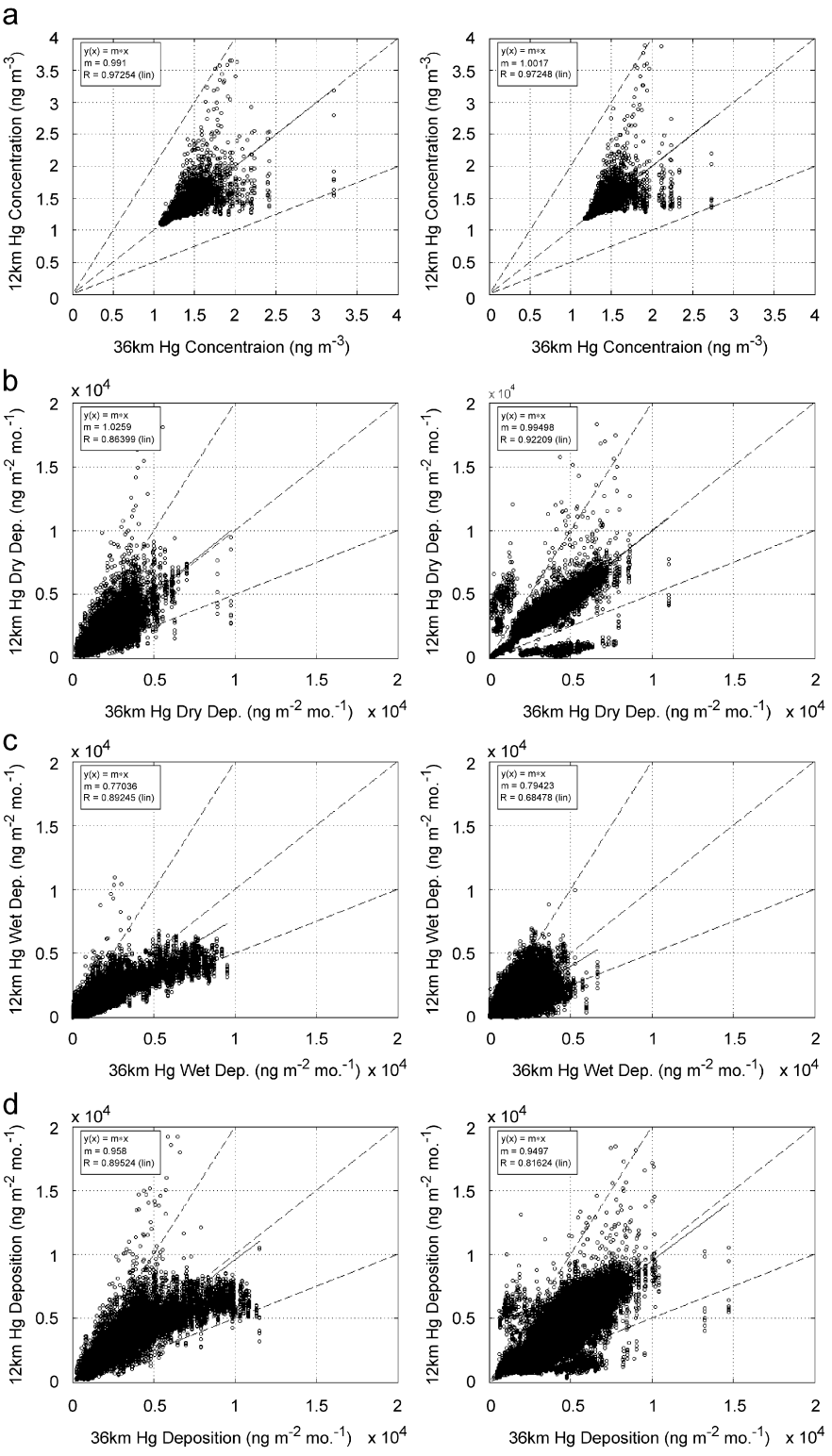

Fig. 3. Comparisons of simulation results at 36 and 12 km spatial resolution in January 2001 (left) and July 2001 (right): (a) monthly average total concentration, (b) monthly accumulated dry deposition, (c) monthly accumulated wet deposition, and (d) monthly accumulated total deposition.

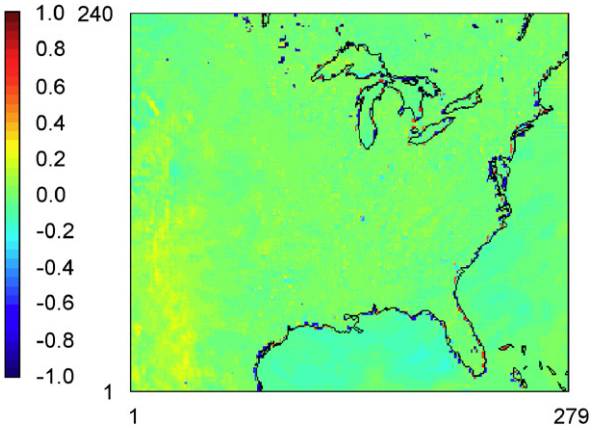

Fig. 4. Ratio of 12–36 km mercury dry depositions in July 2001 (logarithmical value) showing the locations with large discrepancy at different grid resolutions.

resolution also causes the higher mercury deposition near major emission sources. Although this may better represent the concentration and deposition near the emission sources, the benefit is associated with a higher computational cost.

3.2. Boundary and initial conditions

Model results (July 2001) using different concentrations of GEM, RGM and PHg in BC and IC are shown in Table 2. The statistics in Table 2 are obtained from all grid cells of the CONUS 36 km domain. The effect of BC on the model results is shown in Figs. 5 and 6. For better visualization of the data variability, the *Y*-axis of Fig. 5 was cropped from the top and the maximum for each sensitivity case is shown in Table 2. The outliers and extreme outliers in each box plot in Fig. 5 represent the high concentration (Fig. 5a) and dry deposition (Fig. 5b) near large anthropogenic sources and/or high wet deposition (Fig. 5c) at locations with large precipitation. The GEM concentration in BC directly affects the mass of mercury entering the domain. This leads to a difference in the reaction and deposition rates. From Fig. 5 and Table 2, the monthly average of total mercury concentration, and the accumulated dry deposition and wet deposition all increase linearly with respect to GEM concentration. An increase of $1\,ng\,m^{-3}$ of GEM in BC results in an increase of $0.81\,ng\,m^{-3}$ in the monthly average of total mercury concentration and $1270\,ng\,m^{-2}$ in the accumulated total deposition ($r^2>0.99$) for the July 2001 simulation. During the simulation, the mercury originally in the domain can be quickly replaced by the mercury inflow from the boundaries. Since mercury deposition is mainly driven by GEM oxidation chemistry (Lin et al., 2007) and the oxidation of GEM is not an important sink of atmospheric oxidants (Lin and Pehkonen, 1998), the increased GEM concentration in BC proportionally increases the amount of GEM oxidized in the domain.

The influence of RGM and PHg in BC on model results is negligible for the most part of the domain (Fig. 5), partly because the concentrations of RGM and PHg in BC are much smaller (about 2% of GEM concentration). Similar results were also reported by Pai et al. (1999). However, RGM and PHg in BC do have an impact on the simulated dry and wet deposition in the vicinity of domain boundaries, illustrated in Fig. 6 as the monthly average ratios of base-case deposition to the sensitivity cases' deposition. The RGM in BC does not change monthly average concentration (Fig. 6a), but has a strong effect, up to a factor of 11, on monthly accumulated dry deposition (Fig. 6b), wet deposition (Fig. 6c), and total deposition (Fig. 6d) near the domain boundaries for up to 20 grid cells (~720 km) into the domain. In the simulation period (July 2001), the prevailing winds are mostly westerly; therefore, the impact of the RGM boundary condition is more important in the west of the domain. The effect of PHg in BC sensitivity cases shows a similar but weaker trend compared to that of RGM. The impact on dry deposition is negligible because PHg is associated with fine particulate which has a much smaller dry deposition velocity compared to that of RGM. The primary removal mechanism of PHg is through scavenging into the droplet followed by wet removal (Lin et al., 2007).

Figs. 7–9 show the effect of IC on the model results. The effects of mercury concentration in IC on sensitivity test are similar to the effects of BC but to a less extent. The GEM concentration in IC has the greatest effect on the simulated total concentration compared to the cases of RGM and PHg (Fig. 7a). The model response to the change of GEM concentration in IC is also very linear ($r^2>0.99$, an increase of $1\,ng\,m^{-3}$ of GEM in IC results in an increase of $0.14\,ng\,m^{-3}$ in the monthly average of total mercury concentration and $250\,ng\,m^{-2}\,mo^{-1}$ in the accumulated deposition), mainly from the first few days of simulation. RGM and PHg concentrations in IC do not appear to be important (<3% forcing in both concentration and deposition, Fig. 7 and Table 2). Fig. 8 shows the impact of

Table 2
Model statistics from BC and IC experiments for all the grid cells in the CONUS domain

	Base-case	GEM = 0	GEM = 1	GEM = 2	RGM = 0	PHg = 0
BC ($ng\,m^{-3}$)						
Simulated total mercury concentration ($ng\,m^{-3}$)						
Max	8.68	7.73	8.23	9.05	8.63	8.66
Upper quartile	1.49	0.45	1.75	1.99	1.46	1.48
Median	1.47	0.31	1.13	1.94	1.44	1.46
Lower quartile	1.45	0.20	1.08	1.87	1.42	1.45
Min	1.35	0.06	1.01	1.69	1.31	1.35
Simulated monthly dry deposition of mercury ($ng\,m^{-2}\,mo^{-1}$)						
Max	83,993	74,801	79,650	87,601	83,494	83,839
Upper quartile	2432	849	1952	3059	2109	2419
Median	1808	617	1463	2260	1570	1798
Lower quartile	517	215	428	625	396	505
Min	28	18	24	33	14	27
Simulated monthly wet deposition of mercury ($ng\,m^{-2}\,mo^{-1}$)						
Max	6174	4954	5698	7823	5689	6015
Upper quartile	1465	586	1206	1811	1283	1393
Median	755	323	628	923	640	695
Lower quartile	384	171	322	461	302	340
Min	0	0	0	0	0	0
Simulated monthly total deposition of mercury ($ng\,m^{-2}\,mo^{-1}$)						
Max	89,446	77,405	84,837	94,683	88,823	89,132
Upper quartile	3386	1325	2754	4228	2983	3303
Median	2865	1020	2321	3568	2430	2789
Lower quartile	1967	726	1614	2396	1420	1856
Min	49	30	52	63	34	41
IC ($ng\,m^{-3}$)						
Simulated total mercury concentration ($ng\,m^{-3}$)						
Max	8.68	8.54	8.62	8.76	8.66	8.68
Upper quartile	1.49	1.37	1.45	1.60	1.48	1.49
Median	1.47	1.28	1.41	1.56	1.46	1.47
Lower quartile	1.45	1.15	1.37	1.51	1.45	1.45
Min	1.35	0.94	1.26	1.41	1.33	1.35
Simulated monthly dry deposition of mercury ($ng\,m^{-2}\,mo^{-1}$)						
Max	83,993	82,645	83,441	84,737	83,779	83,958
Upper quartile	2432	2151	2346	2548	2391	2,429
Median	1808	1531	1732	1906	1760	1,806
Lower quartile	517	465	502	534	500	516
Min	28	27	28	29	28	28
Simulated monthly wet deposition of mercury ($ng\,m^{-2}\,mo^{-1}$)						
Max	6174	6001	6005	6613	6011	6142
Upper quartile	1465	1241	1398	1548	1424	1444
Median	755	668	729	789	733	744
Lower quartile	384	341	373	396	370	376
Min	0	0	0	0	0	0
Simulated monthly total deposition of mercury ($ng\,m^{-2}\,mo^{-1}$)						
Max	89,446	88,612	89,137	89,627	89,354	89,393
Upper quartile	3386	2969	3259	3562	3312	3369
Median	2865	2494	2761	2992	2796	2851
Lower quartile	1967	1741	1916	2024	1906	1948
Min	49	48	49	49	49	49

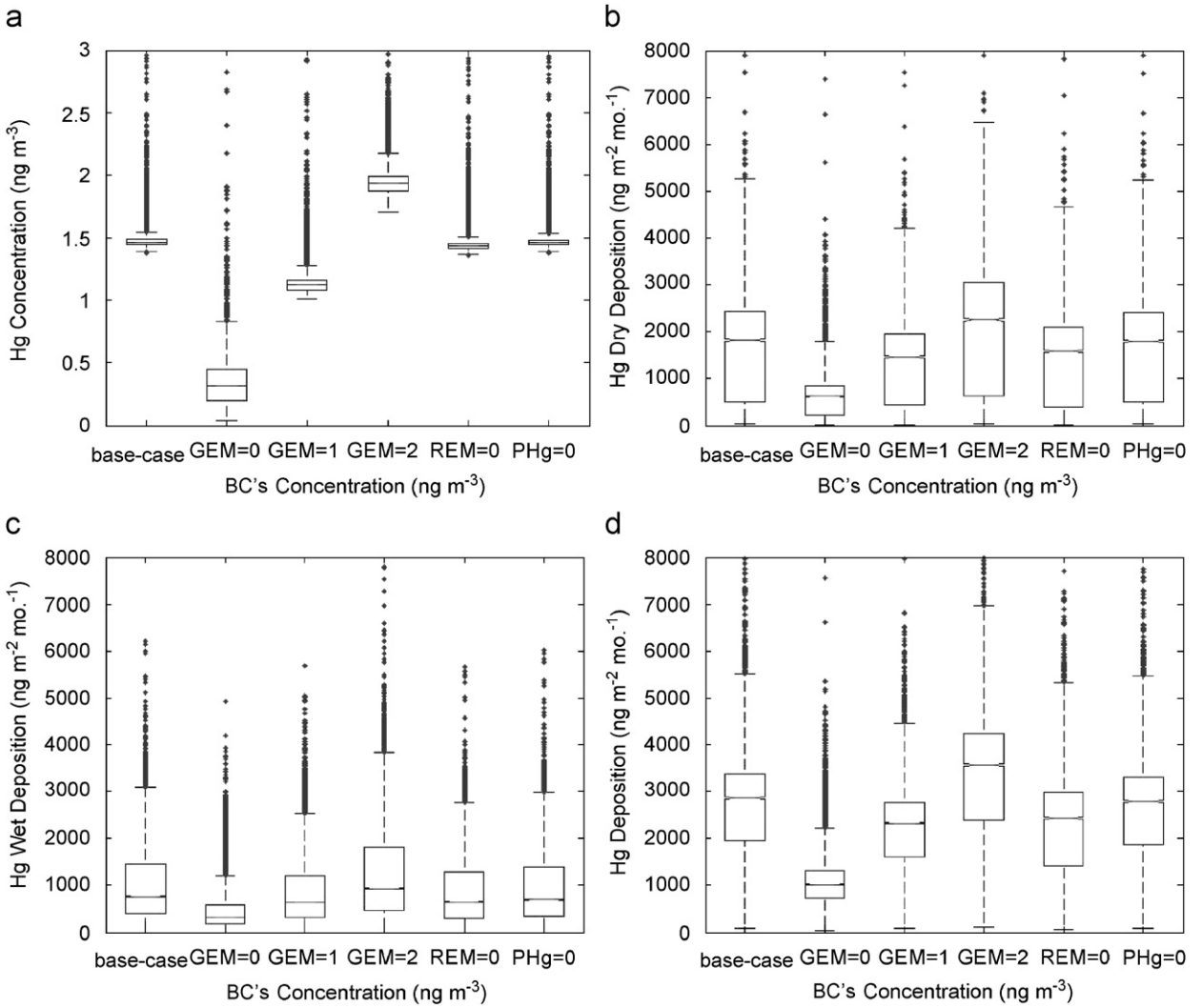

Fig. 5. Effect of mercury species concentration in BC on simulation results in July 2001: (a) monthly average total concentration, (b) monthly accumulated dry deposition, (c) monthly accumulated wet deposition, and (d) monthly accumulated total deposition.

RGM and PHg in IC as the monthly average ratios of base-case results to the sensitivity case results. As seen, RGM in IC have some impact (up to a factor of 2) on both dry and wet deposition; while PHg have a small effect on the wet deposition. The locations with high ratios of monthly wet deposition (Fig. 8c) are caused by the precipitation scavenging of RGM and PHg in the IC during the first few days of the modeling period.

Since the impact of IC is mainly from the first few days of simulation, the day-by-day variation of the peak ratio shown in Fig. 8 was investigated, which is plotted in Fig. 9. The peak ratios of model results caused by removing RGM (Fig. 9a) and PHg (Fig. 9b) in IC gradually reach 1.0 after only a week of simulation. This indicates that the mercury mass in the domain can be replaced by the mercury inflow from boundary conditions within a week. In other words, a model spin-up time of 7 days or longer can eliminate the impact caused by RGM and PHg concentrations in IC in the CONUS domain, and this result should also apply to other regional domains with a similar prevailing wind speed.

From the above analysis, it is clear that a realistic GEM field in BC and IC is important for atmospheric mercury simulation in a regional domain. The increase of GEM concentration in BC and IC can lead to linear increases of both concentration and deposition, though the impact from BC is much

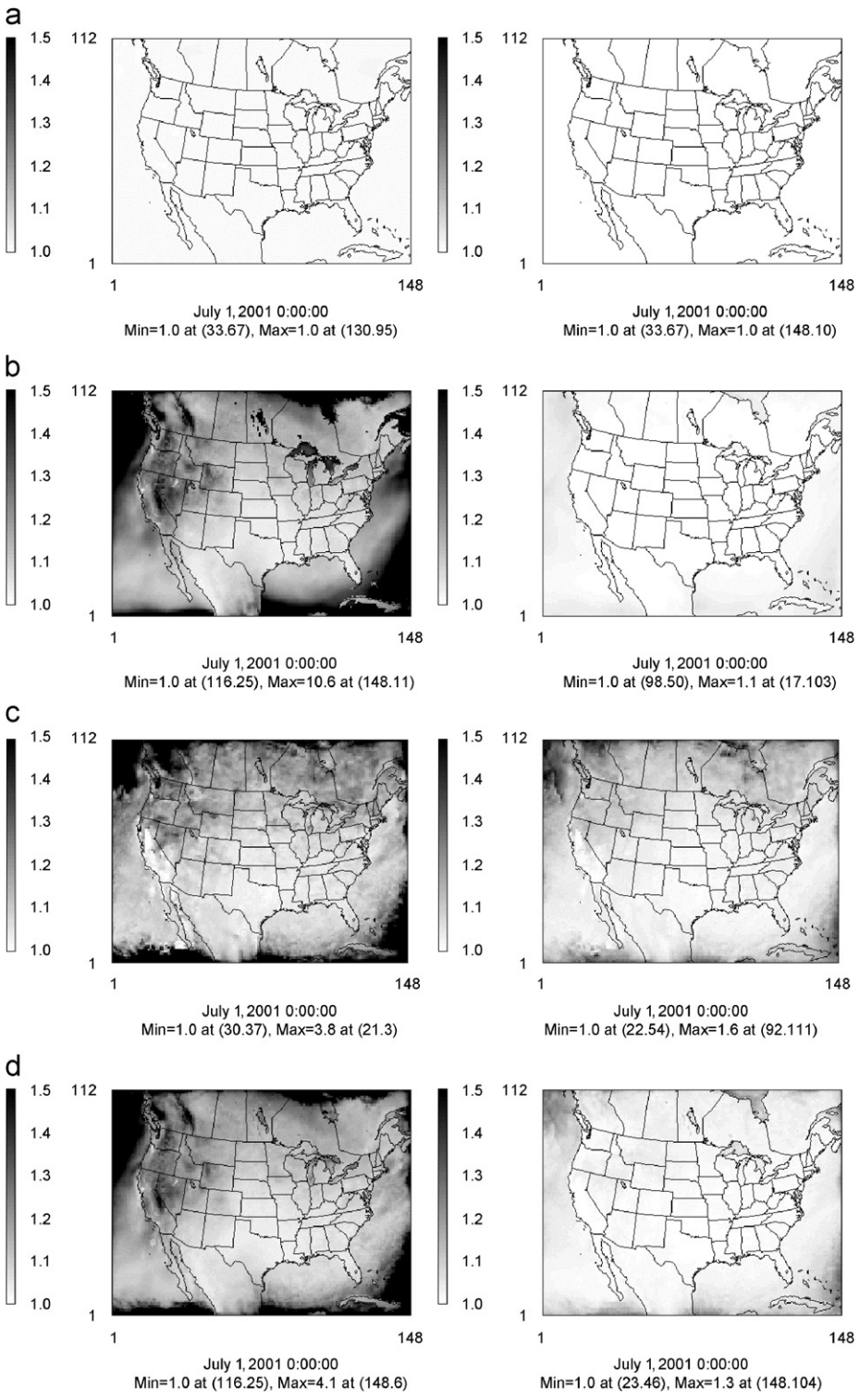

Fig. 6. Monthly average ratios of base-case results to BC sensitivity case results of RGM (left) and PHg (right): (a) monthly average total concentration, (b) monthly accumulated dry deposition, (c) monthly accumulated wet deposition, and (d) monthly accumulated total deposition.

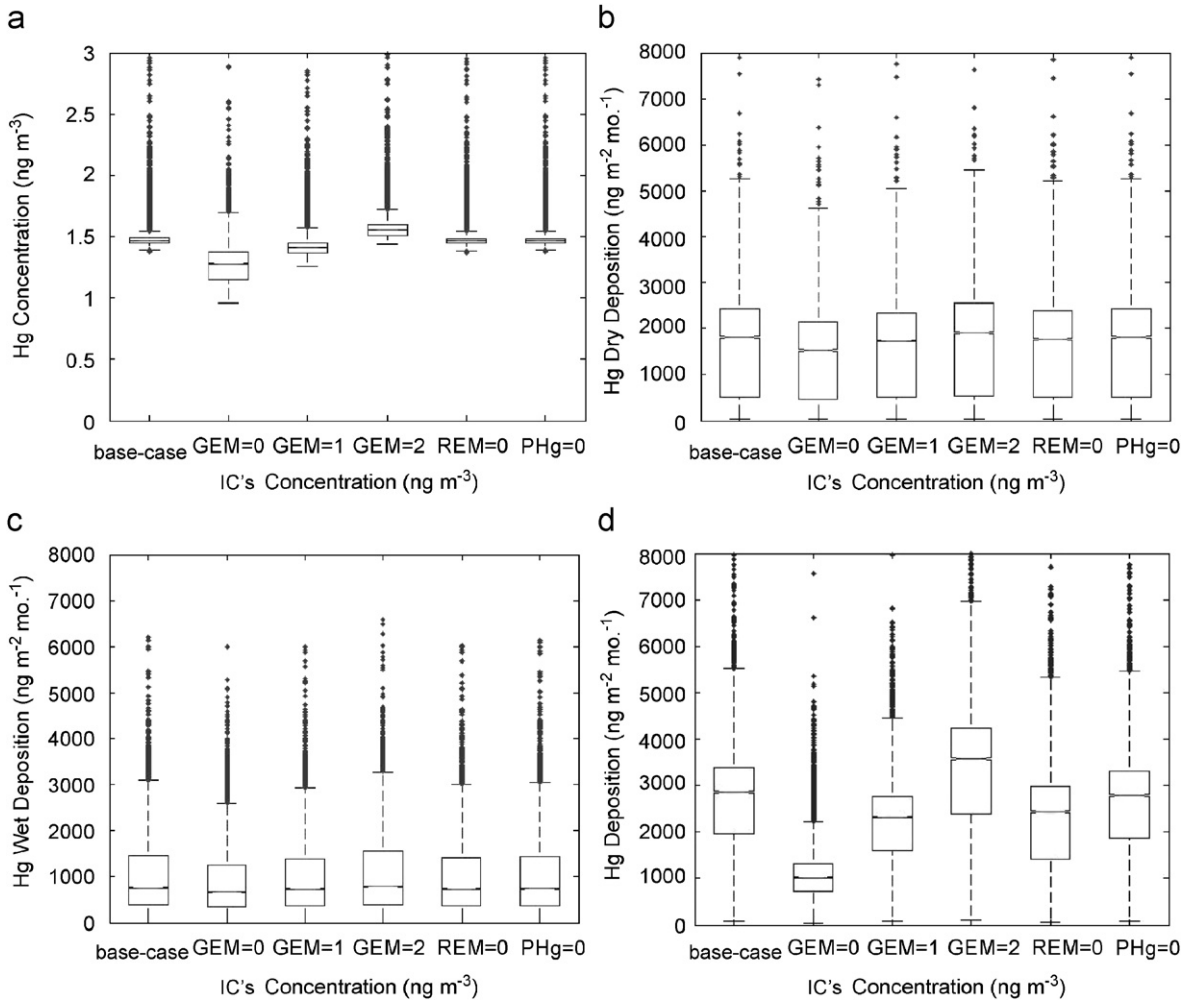

Fig. 7. Effect of mercury species concentration in IC on simulation results in July 2001: (a) monthly average total concentration, (b) monthly accumulated dry deposition, (c) monthly accumulated wet deposition, and (d) monthly accumulated total deposition.

more predominant. Since the use of global model output for BC and IC in regional simulations can provide a better representation of GEM distribution, it is advisable to implement nesting simulations whenever possible although global models also have their own uncertainties.

3.3. Alternative Hg(II) reduction mechanisms

The simulated mercury wet depositions in July 2001 using CMAQ-Hg 4.5.1 are illustrated in Fig. 10a, visualized with the MDN measured wet deposition. In comparison with MDN observations, the model underestimated wet depositions (slope = 0.66, $r^2 = 0.76$) (Lin et al., 2007), while simulated precipitation correlated well with measured MDN measurements (slope = 1.07, $r^2 = 0.87$). The wet deposition is much enhanced when aqueous Hg(II) reduction by HO_2 is removed (Fig. 10b), with an increase by more than a factor of 2 (from 0.66 to 1.54 times of the MDN-measured wet depositions). Recent studies (Lin et al., 2007; Seigneur et al., 2006; Sillman et al., 2007) also showed that wet depositions and RGM concentrations would be increased drastically, and GEM concentrations would be lowered by a factor of 2–4 if the aqueous HO_2 reduction mechanism is removed. Therefore, if the aqueous reduction of Hg(II) by HO_2 is a reality, it will be the most important reduction pathway of GEM in the atmosphere.

Two sets of sensitivity simulation were performed using two alternative reduction mechanisms in gaseous phase, i.e., reduction by CO and photoreduction

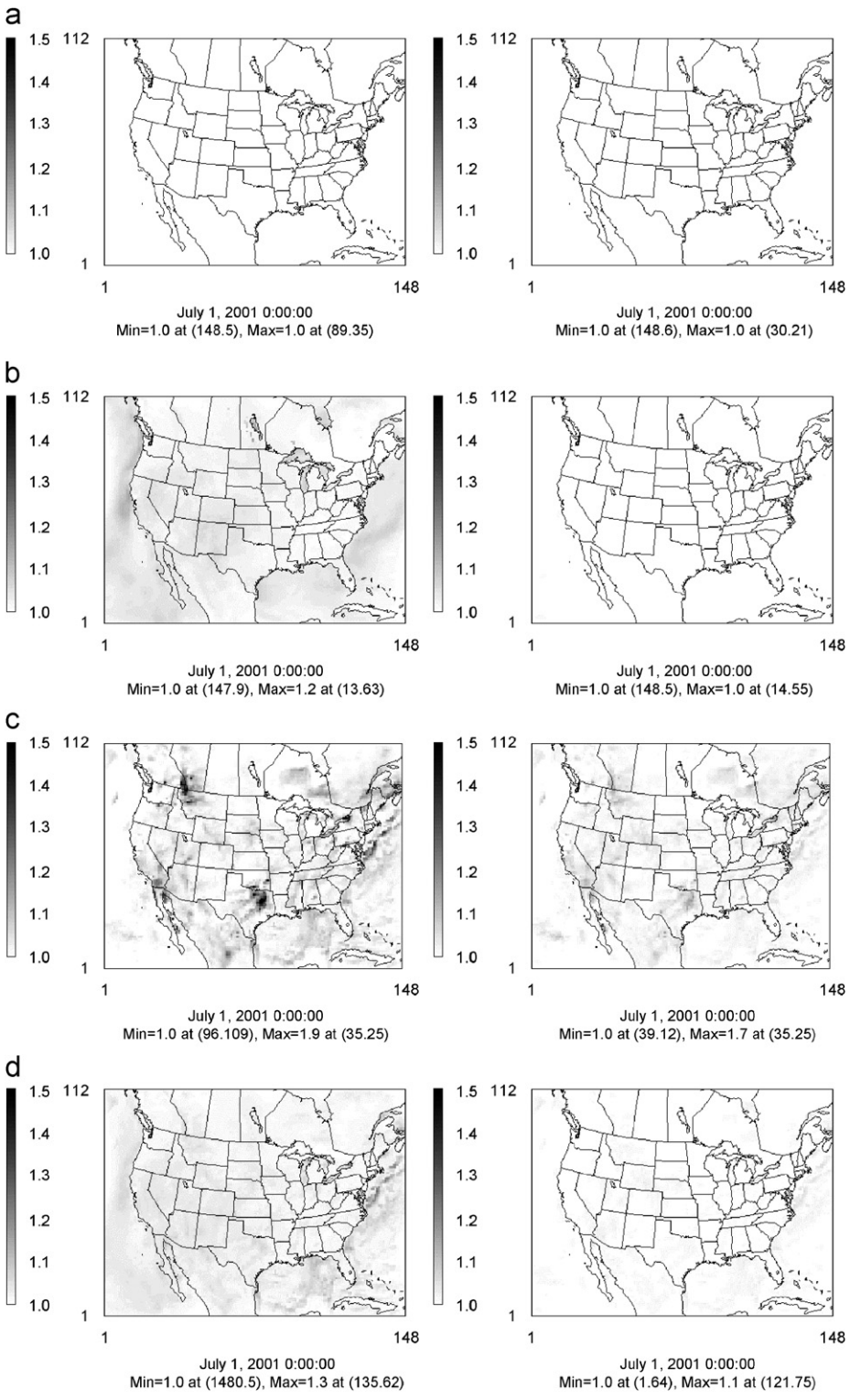

Fig. 8. Monthly average ratios of base-case results to IC sensitivity-case results for RGM (left) and PHg (right): (a) monthly average total concentration, (b) monthly accumulated dry deposition, (c) monthly accumulated wet deposition, and (d) monthly accumulated total deposition.

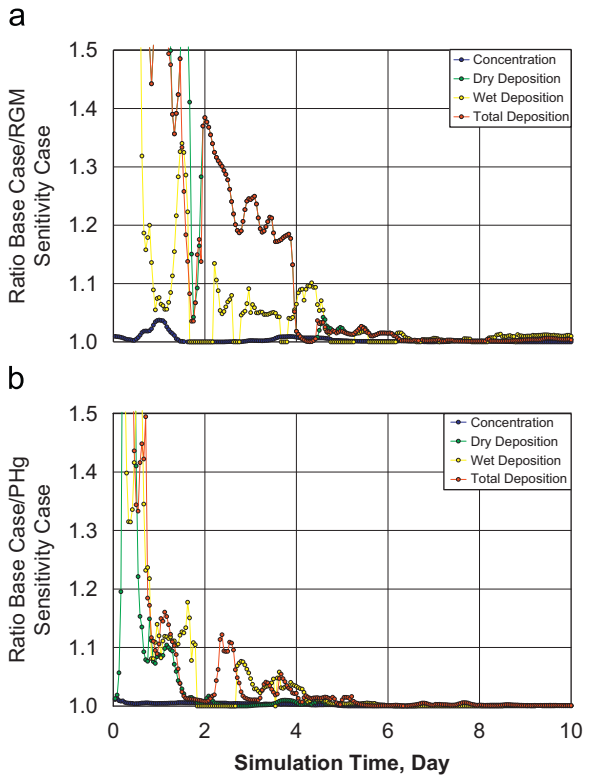

Fig. 9. Variation of the day-by-day peak ratio of base-case results to IC sensitivity-case results in the domain for (a) RGM and (b) PHg.

of RGM. In the simulation, the alternative mechanisms were implemented one at a time, and the reduction pathway via HO_2 was turned off. The CO reduction rates were varied from 10^{-20} to $10^{-14}\,cm^3\,molecule^{-1}\,s^{-1}$ and the RGM photoreduction rates were varied from 10^{-7} to $10^{-1}\,s^{-1}$. The corresponding simulated wet depositions were plotted against the MDN data in Figs. 11 and 12. It should be noted that Figs. 11 and 12 are shown in log scale is for better data visualization. The regression statistics in both figures were obtained from the data in arithmetic scale.

Implementing a rate of $5\times10^{-18}cm^3\,molecule^{-1}\,s^{-1}$ for the hypothetical RGM reduction by CO gives improved model agreement with the MDN-measured deposition (slope = 0.97, $r^2 = 0.94$, Figs. 10c and 11), as compared to the base-case (slope = 0.66, $r^2 = 0.76$, Fig. 10a). For RGM photoreduction, a first-order rate of $10^{-5}\,s^{-1}$ produces wet deposition results compared favorably to the MDN data (slope = 1.04, $r^2 = 0.94$, Figs. 10d and 11). The second-order rate of $5\times10^{-18}\,cm^3\,molecule^{-1}\,s^{-1}$ (CO as the reductant) is comparable to the empirical reduction rate of $8\times10^{-18}\,cm^3\,molecule^{-1}\,s^{-1}$ (SO_2 as the reductant) reported by Lohman et al. (2006). This is noteworthy since CO is a persistent species and its average concentration is much higher than SO_2 in the atmosphere. Furthermore, elevated SO_2 levels can only be observed near the emission sources due to its relatively short atmospheric lifetime. Therefore, the RGM reduction rate by SO_2 would need to be much greater than the reduction rate by CO to have a similar reduction contribution. An earlier study by Seigneur et al. (2006) has demonstrated that using the rate of $8\times10^{-18}\,cm^3\,molecule^{-1}\,s^{-1}$ (adopted from Lohman et al., 2006) for RGM reduction by SO_2 was not sufficient to replace aqueous Hg(II) reduction by HO_2 in a global model. On the other hand, implementing the reduction of RGM by SO_2 in plume models is perhaps plausible because the concentration of SO_2 in emission plumes is much higher than its ambient concentration, and the higher plume temperature may also facilitate the reduction.

The tested RGM photoreduction rate of $10^{-5}\,s^{-1}$ in this study is significantly lower than the pseudo-first-order reduction rate of $8.3\times10^{-5}\,s^{-1}$ reported by Lohman et al. (2006). A global simulation showed that the use of a pseudo-first-order RGM reduction rate of $4.2\times10^{-5}\,s^{-1}$ (half-rate of Lohman et al., 2006) to replace aqueous Hg(II) reduction by HO_2 is too fast and leads to overestimation of GEM concentrations by a factor of 2 (Seigneur et al., 2006). It should be noted that implementing photoreduction and pseudo-first-order reduction in the model is fundamentally different. The rate of photoreduction varies with solar irradiation and shows diurnal cycle, while the pseudo-first-order RGM reduction is similar to a first-order-decay reaction and does not show diurnal cycle.

The sensitivity of simulated mercury wet deposition to the reduction coefficients is shown in Fig. 13. The implemented reduction mechanisms have little effect on the simulated wet deposition when CO reduction rate is $<1\times10^{-20}\,cm^3\,molecule^{-1}\,s^{-1}$ or RGM photoreduction rate is $<1\times10^{-7}\,s^{-1}$, due to the negligible reduction rate. When CO reduction rate is $>1\times10^{-15}\,cm^3\,molecule^{-1}\,s^{-1}$ or RGM photoreduction rate is $>1\times10^{-2}\,s^{-1}$, the reduction reactions do not have further effect on the simulated wet deposition, either. Under such conditions, the reduction rate is much faster than the oxidation rate, and the oxidized mercury is rapidly reduced back to GEM. This indicates that the simulated deposition is sensitive to a reduction mechanism

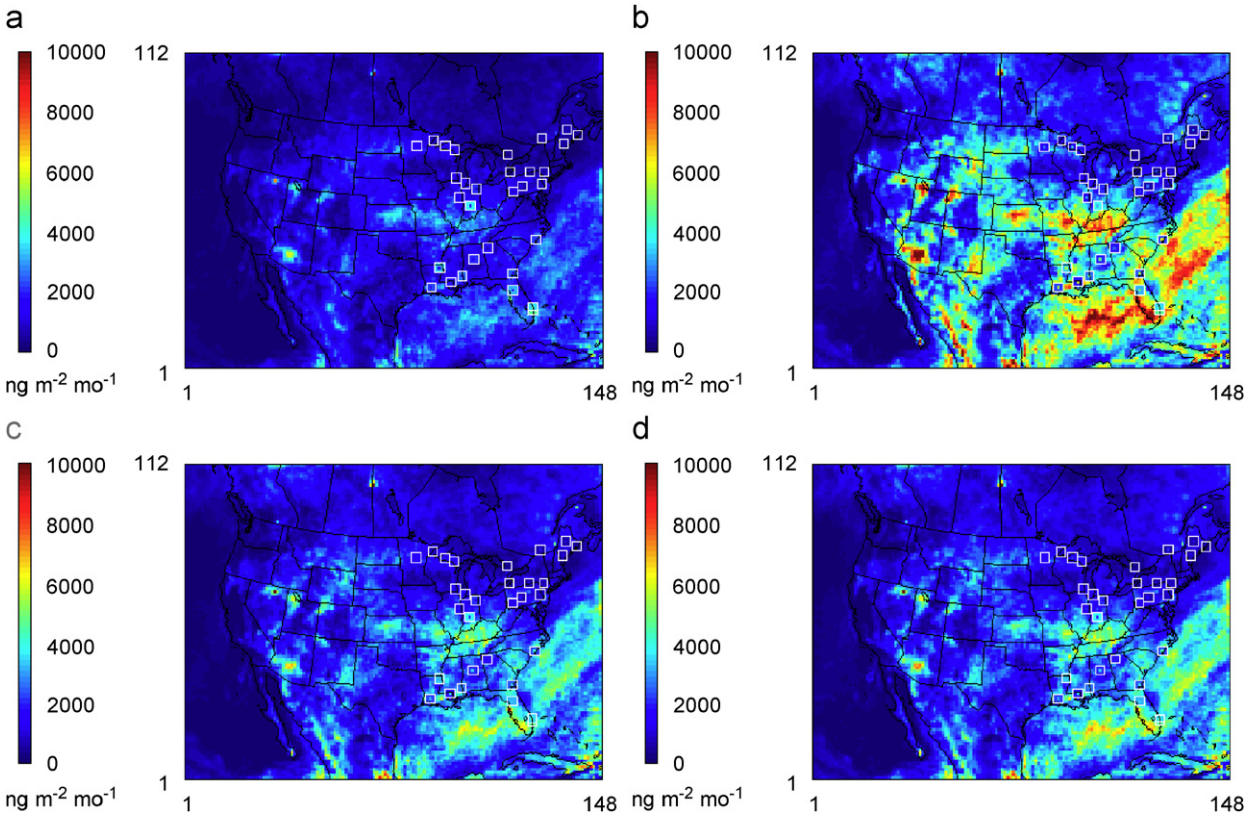

Fig. 10. Simulated mercury wet deposition for (a) base-case, (b) removing the aqueous Hg(II) reduction by HO_2 from mercury chemical mechanisms, (c) using the alternative reduction mechanism of RGM reduction by CO with $k_{CO} = 5 \times 10^{-18}$ cm^3 molecule^{-1} s^{-1}, (d) using the alternative reduction mechanism of RGM photoreduction with $J_{RGM} = 10^{-5}$ s^{-1} (MDN measurements in small boxes). Note that RGM is assigned as the GEM oxidation product for all the cases above.

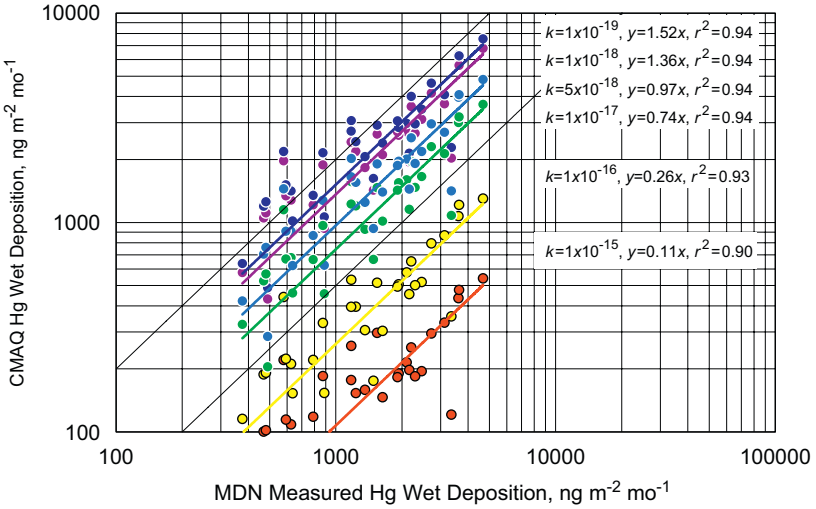

Fig. 11. Scattered plots of simulated versus MDN-measured mercury wet deposition in July 2001 by various rates of RGM reduction by CO. The unit of the rate constant is cm^3 molecule^{-1} s^{-1}.

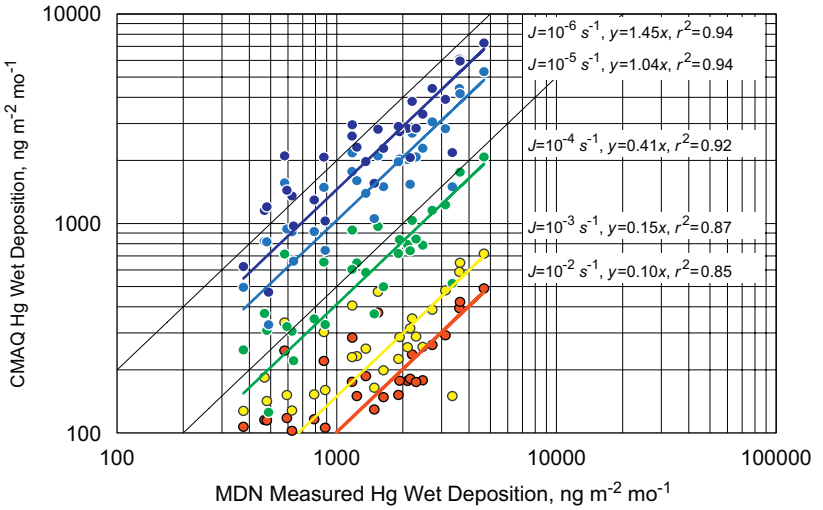

Fig. 12. Scattered plots of simulated versus MDN-measured mercury wet deposition in July 2001 by various rates of RGM photoreduction.

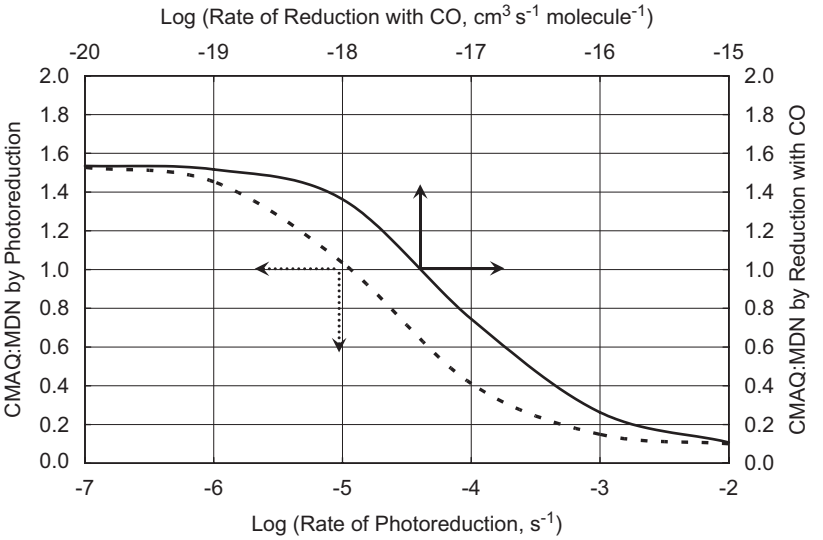

Fig. 13. Ratios of simulated over MDN-measured mercury wet deposition at various reduction rates: solid line for RGM reduction by CO and dashed line for RGM photoreduction.

only when its kinetic parameter falls within a certain range. From Fig. 13, the most sensitive ranges for the RGM photoreduction and reduction by CO are 10^{-6}–$10^{-3}\,s^{-1}$ and 10^{-18}–$10^{-16}\,cm^3\,molecule^{-1}\,s^{-1}$, respectively. If future laboratory kinetic measurements confirm that that these reactions indeed occur, with reaction rates within the sensitive ranges (or other gaseous reduction reactions with similar rates), the reactions will be important for transforming mercury in the atmosphere.

4. Conclusions

In this study, the model response to the boundary and initial conditions of mercury species, model grid resolution (12 km versus 36 km), and alternative Hg(II) reduction mechanisms, i.e., RGM reduction by CO and photoreduction, was investigated. Although model results using the two different resolutions are similar, using the finer spatial resolution better resolves the simulated concentration

and deposition, especially near the major emission sources. The model response to the change of GEM concentration from 0 to $2\,ng\,m^{-3}$ in IC/BC is found to be very linear ($r^2 > 0.99$) based on the results of sensitivity simulation in July 2001, although the effect of IC is much weaker compared to that of BC. RGM and PHg concentrations in BC have a strong impact near domain boundaries for up to 20 grid cells into the CONUS domain. A model spin-up time of 7 days or longer can eliminate the impact of RGM and PHg concentrations in IC in the CONUS domain based on our simulation results.

The results from the sensitivity simulation using two alternative RGM reduction mechanisms, implemented one at a time, that replace the aqueous Hg(II) reduction by HO_2 show considerable improvement in model performance. A second-order rate of $5 \times 10^{-18}\,cm^3\,molecule^{-1}\,s^{-1}$ for RGM reduction by CO, a first-order rate of $1 \times 10^{-5}\,s^{-1}$ for photoreduction of RGM, or a similar rate by any reduction mechanisms in gaseous phase, give significantly better model agreement with MDN-measured deposition. It is also found that the simulated deposition is sensitive to a reduction mechanism only when the rate constant falls within a certain range. The kinetic range predicted by the sensitivity simulation provides a preliminary rate estimate, and further verification by laboratory kinetic studies is needed.

Acknowledgments

The authors would like to acknowledge the funding support from Texas Commission on Environmental Quality (TCEQ work order number: 64582-06-15), the USEPA Office of Air Quality Planning and Standards (RTI subcontract number: 6-321-0210288) and Texas Air Research Center (TARC project number: 077LUB0976). A portion of the research presented here was performed under the Memorandum of Understanding between the US Environmental Protection Agency (EPA) and the US Department of Commerce's National Oceanic and Atmospheric Administration (NOAA) and under agreement number DW13921548. This work constitutes a contribution to the NOAA Air Quality Program. Although it has been reviewed by EPA and NOAA and approved for publication, it does not necessarily reflect their policies or views. The thoughtful comments from the anonymous reviewers are gratefully acknowledged.

References

Abbott, M.L., Lin, C.-J., Martian, P., Einerson, J.J., 2008. Atmospheric mercury near Salmon Falls Creek Reservoir in Southern Idaho. Applied Geochemistry 23 (3).

Aldrich Chemical Company, 2006. Handbook of Fine Chemicals. Sigma-Aldrich Corporation, Milwaukee, WI.

Beckman, A.O., McCullough, J.D., Crane, R.A., 1948. Microdetermination of carbon monoxide in air. Analytical Chemistry 20 (7), 674–677.

Bullock, O.R., Brehme, K.A., 2002. Atmospheric mercury simulation using the CMAQ model: formulation description and analysis of wet deposition results. Atmospheric Environment 36, 2135–2146.

Byun, D.W., Ching, J.K.S., 1999. Science algorithms of the EPA Models-3 Community Multiscale Air Quality (CMAQ) modeling system. Rep EPA-600/R-99/030. Office of Research and Development, US Environmental Protection Agency, Washington, DC.

Fay, I.W., Seeker, A.F., 1903. Reducibility of some metallic oxides by hydrogen and carbon monoxide. Journal of the American Chemical Society 25, 641–647.

Fulkerson, M., Nnadi, F.N., 2006. Predicting mercury wet deposition in Florida: a simple approach. Atmospheric Environment 40, 3962–3968.

Gårdfeldt, K., Jonsson, M., 2003. Is bimolecular reduction of Hg(II) complexes possible in aqueous systems of environmental importance? The Journal of Physical Chemistry A 107, 4478–4482.

Gbor, P.K., Wen, D., Meng, F., Yang, F., Zhang, B., Sloan, J.J., 2006. Improved model for mercury emission, transport and deposition. Atmospheric Environment 40, 973–983.

Gbor, P.K., Wen, D., Meng, F., Yang, F., Sloan, J.J., 2007. Modeling of mercury emission, transport and deposition in North America. Atmospheric Environment 41, 1135–1149.

Grell, G.A., Dudhia, J., Stauffer, D.R., 1994. A description of the fifth-generation Penn State/NCAR Mesoscale Model (MM5). NCAR Tech Note TN-398 + STR, 122pp.

Jacobson, M.Z., 1999. Fundamentals of Atmospheric Modeling. Cambridge University Press, 672pp.

Kawano, T., Tsuboi, N., Tsujii, H., Sugiyama, T., Asakura, Y., Uda, T., 2004. Stability test and improvement of hydrogen analyzer with trace reduction detector. Journal of Chromatography A 1023 (1), 123–127.

Kawano, T., Tsuboi, N., Tsujii, H., Asakura, Y., Uda, T., 2005. Isotopic separation analysis of infinitesimal concentrations of hydrogen using trace reduction detector. Fusion Science and Technology 48 (1), 405–408.

Kellerhals, M., Beauchamp, S., Belzer, W., Blanchard, P., Froude, F., Harvey, B., McDonald, K., Pilote, M., Poissant, L., Puckett, K., Schroeder, B., Steffen, A., Tordon, R., 2003. Temporal and spatial variability of total gaseous mercury in Canada: results from the Canadian atmospheric mercury measurement network (CAMNet). Atmospheric Environment 37, 1003–1011.

Lin, C.-J., Pehkonen, S.O., 1998. Two-phase model of mercury chemistry in the atmosphere. Atmospheric Environment 32, 2543–2558.

Lin, C.J., Pehkonen, S.O., 1999. The chemistry of atmospheric mercury: a review. Atmospheric Environment 33, 2067–2079.

Lin, X., Tao, Y., 2003. A numerical modelling study on regional mercury budget for eastern North America. Atmospheric Chemistry and Physics 3, 535–548.

Lin, C.J., Lindberg, S.E., Ho, T.C., Jang, C., 2005. Development of a processor in BEIS3 for estimating vegetative mercury emission in the continental United States. Atmospheric Environment 39, 7529–7540.

Lin, C.J., Pongprueksa, P., Lindberg, S.E., Pehkonen, S.O., Byun, D., Jang, C., 2006a. Scientific uncertainties in atmospheric mercury models I: model science evaluation. Atmospheric Environment 40, 2911–2928.

Lin, C.J., Pongprueksa, P., Vanjani, T., Ho, T.C., Chu, H.W., Jang, C., Braverman, T., Streets, D.G., Fu, J.S., 2006b. Trans-Pacific chemical transport of mercury: sensitivity analysis on potential Asian emission contribution to mercury deposition in North America using CMAQ-Hg. In: Proceedings of the 5th CMAS Conference, Research Triangle Park, NC, 16–18 October 2006.

Lin, C.J., Pongprueksa, P., Bullock, O.R., Lindberg, S.E., Pehkonen, S.O., Jang, C., Braverman, T., Ho, T.C., 2007. Scientific uncertainties in atmospheric mercury models II: sensitivity analysis in the CONUS Domain. Atmospheric Environment 41, 6544–6560.

Lohman, K., Seigneur, C., Edgerton, E., Jansen, J., 2006. Modeling mercury in power plant plumes. Environmental Science and Technology 40 (12), 3848–3854.

McCullough, J.D., Crane, R.A., Beckman, A.O., 1947. Determination of carbon monoxide in air by use of red mercuric oxide. Analytical Chemistry 19 (12), 999–1002.

Pai, P., Karamchandani, P., Seigneur, C., Allan, M.A., 1999. Sensitivity of simulated atmospheric mercury concentrations and deposition to model input parameters. Journal of Geophysical Research-Atmospheres 104 (D11), 13855–13868.

Pai, P., Karamchandani, P., Seigneur, C., 2000. On artificial dilution of point source mercury emissions in a regional atmospheric model. Science of the Total Environment 259 (1–3), 159–168.

Pehkonen, S.O., Lin, C.J., 1998. Aqueous photochemistry of mercury with organic acids. Journal of the Air and Waste Management Association 48 (2), 144–150.

Pleim, J.E., Byun, D.W., 2004. Application of a new land-surface, dry deposition, and PBL model in the models—3 Community Multi-Scale Air Quality (CMAQ) model system. In: Gryning, S., Schiermeier, F.A. (Eds.), Air Pollution Modeling and Its Application XIV. Kluwer Academic Publishers, pp. 297–305.

Seigneur, C., Wrobel, J., Constantinou, E., 1994. A chemical kinetic mechanism for atmospheric inorganic mercury. Environmental Science and Technology 28 (9), 1589–1597.

Seigneur, C., Karamchandani, P., Vijayaraghavan, K., Lohman, K., Shia, R.L., Levin, L., 2003. On the effect of spatial resolution on atmospheric mercury modeling. Science of the Total Environment 304 (1–3), 73–81.

Seigneur, C., Vijayaraghavan, K., Lohman, K., 2006. Atmospheric mercury chemistry: sensitivity of global model simulations to chemical reactions. Journal of Geophysical Research-Atmospheres 111 (D22306).

Selin, N.E., Jacob, D.J., Park, R.J., Yantosca, R.M., Strode, S., Jaeglé, L., Jaffe, D., 2007. Chemical cycling and deposition of atmospheric mercury: global constraints from observations. Journal of Geophysical Research-Atmospheres 112 (D02308).

Sillman, S., Marsik, F.J., Al-Wali, K.I., Keeler, G.J., Landis, M.S., 2007. Reactive mercury in the troposphere: model formation and results for Florida, the northeastern US and the Atlantic Ocean. Journal of Geophysical Research-Atmospheres in press, doi:10.1029/2006JD008227.

Tanaka, P.L., Allen, D.T., McDonald-Buller, E.C., Chang, S.H., Kimura, Y., Mullins, C.B., Yarwood, G., Neece, J.D., 2003. Development of a chlorine mechanism for use in the carbon bond IV chemistry model. Journal of Geophysical Research-Atmospheres 108 (D4).

Temme, C., Blanchard, P., Steffen, A., Banic, C., Beauchamp, S., Poissant, L., Tordon, R., Wiens, B., 2007. Trend, seasonal and multivariate analysis study of total gaseous mercury data from the Canadian atmospheric mercury measurement network (CAMNet). Atmospheric Environment 41, 5423–5441.

Walcek, C., De Santis, S., Gentile, T., 2003. Preparation of mercury emissions inventory for eastern North America. Environmental Pollution 123, 375–381.

Zender, C.S., 2007. Analysis of Self-describing Gridded Geoscience Data with netCDF Operators (NCO), Environmental Modelling and Software, on-line: http://dust.ess.uci.edu/ppr/pprZen07.pdf.